Monomeric and fibrillar α-synuclein exert opposite effects on the catalytic cycle that promotes the proliferation of Aβ42 aggregates

Sean Chia[a,1], Patrick Flagmeier[a,1], Johnny Habchi[a,1], Veronica Lattanzi[b], Sara Linse[b], Christopher M. Dobson[a], Tuomas P. J. Knowles[a], and Michele Vendruscolo[a,2]

[a]Centre for Misfolding Diseases, Department of Chemistry, University of Cambridge, Cambridge CB2 1EW, United Kingdom; and [b]Department of Biochemistry and Structural Biology, Center for Molecular Protein Science, Lund University, 221 00 Lund, Sweden

Edited by Solomon H. Snyder, Johns Hopkins University School of Medicine, Baltimore, MD, and approved June 6, 2017 (received for review January 5, 2017)

The coaggregation of the amyloid-β peptide (Aβ) and α-synuclein is commonly observed in a range of neurodegenerative disorders, including Alzheimer's and Parkinson's diseases. The complex interplay between Aβ and α-synuclein has led to seemingly contradictory results on whether α-synuclein promotes or inhibits Aβ aggregation. Here, we show how these conflicts can be rationalized and resolved by demonstrating that different structural forms of α-synuclein exert different effects on Aβ aggregation. Our results demonstrate that whereas monomeric α-synuclein blocks the autocatalytic proliferation of Aβ42 (the 42-residue form of Aβ) fibrils, fibrillar α-synuclein catalyses the heterogeneous nucleation of Aβ42 aggregates. It is thus the specific balance between the concentrations of monomeric and fibrillar α-synuclein that determines the outcome of the Aβ42 aggregation reaction.

Alzheimer's disease | Parkinson's disease | dementia with Lewy bodies | chemical kinetics | amyloid fibrils

Alzheimer's disease (AD) and Parkinson's disease (PD) have been closely associated with the misfolding and aggregation of Aβ into amyloid plaques and of α-synuclein into Lewy bodies, respectively (1–12). In other situations, as for example in the case of dementia with Lewy bodies (DLB), amyloid plaques and Lewy bodies are observed together, and parts of the sequence of α-synuclein are found to constitute the nonamyloid component (NAC) of amyloid plaques (13–17). Therefore, Aβ may be able to interact with α-synuclein, especially considering that α-synuclein can also be found in the extracellular space where Aβ deposits are typically observed (11). Strikingly, however, conflicting reports have shown opposing effects of α-synuclein on the aggregation of Aβ. Although it has been shown that α-synuclein promotes Aβ aggregation (18–20), recent in vivo studies have demonstrated that the coexpression of α-synuclein and Aβ in a transgenic mouse model reduces the load of amyloid plaques (21), and that the knockout of α-synuclein from a mouse model of AD leads to an increase in the formation of amyloid plaques (22). These apparently conflicting results suggest a complex scenario that requires a detailed understanding of the mechanism underlying the interactions between α-synuclein and Aβ.

Such an understanding can be achieved in a quantitative manner through the application of highly reproducible chemical kinetic assays that allow the rates of individual microscopic processes during the aggregation process to be measured (23–26). In the case of Aβ42, this kinetic assay allowed the definition of a network of pathways from reactants to products that has provided a detailed understanding of the self-assembly process of this peptide (24, 27, 28). As a result, fibril-catalyzed secondary nucleation was found to be the dominant mechanism that is responsible for the formation of Aβ42 aggregates, in which a positive-feedback loop leads to the generation of oligomers from the nucleation of Aβ42 monomers at the surface of fibrils (24). Furthermore, chemical kinetics also allowed the characterization of the effects of extrinsic factors on the aggregation of Aβ42 at a microscopic level. In particular, molecular chaperones were found to suppress amyloid formation by binding to distinct species and subsequently affecting different microscopic steps in the aggregation process (28–30). In the same vein, small molecules and antibodies have been developed to inhibit specific steps in the aggregation of Aβ42 (31–33). These data have proven the efficacy of chemical kinetics in describing the effects of extrinsic factors on the aggregation of Aβ42 in a highly sensitive manner. We therefore used in the present study the substantial advances in chemical kinetics to unravel the role of α-synuclein on Aβ42 aggregation.

Results

Monomeric α-Synuclein Inhibits Aβ42 Secondary Nucleation. We first carried out a global kinetic analysis of Aβ42 aggregation in the absence and presence of monomeric α-synuclein (Fig. 1 *A*–*C* and Fig. S1*A*) (24). These results indicated that monomeric α-synuclein delayed substantially the overall rates of formation of Aβ42 fibrils in a concentration-dependent manner (Fig. 1 *A*–*C* and Fig. S1*A*). This inhibitory effect was found to reach saturation in the presence of about 2 molar equivalents of α-synuclein (Fig. S1*A*).

We next carried out a quantitative analysis by matching the aggregation profiles on the basis of rate laws derived from a master equation that relate the macroscopic time evolution of the quantity of fibrils that are formed during the aggregation reaction to the rate constants of the different microscopic events (34, 35). Using this approach, the aggregation profiles in the presence of α-synuclein

Significance

A variety of neurodegenerative disorders, such as Alzheimer's and Parkinson's diseases, involve the aggregation of Aβ and α-synuclein. These two proteins can influence each other in a complex manner, which has so far prevented firm conclusions to be established about whether, in particular, α-synuclein promotes or inhibits Aβ aggregation. By exploiting a highly quantitative chemical kinetics approach, we show that α-synuclein monomers inhibit Aβ42 aggregation by binding to Aβ42 fibrils, thereby preventing them from catalysing the nucleation of further Aβ42 aggregates. By contrast, α-synuclein fibrils do just the opposite, as they catalyse the nucleation of Aβ42 aggregates. These results show how approaches based on chemical kinetics can provide essential insights into complex aggregation phenomena and illustrate the nature of the interaction between Aβ and α-synuclein.

Author contributions: S.C., P.F., J.H., S.L., C.M.D., T.P.J.K., and M.V. designed research; S.C., P.F., J.H., V.L., and S.L. performed research; S.C., P.F., J.H., V.L., and S.L. contributed new reagents/analytic tools; S.C., P.F., J.H., S.L., C.M.D., T.P.J.K., and M.V. analyzed data; and S.C., P.F., J.H., S.L., C.M.D., T.P.J.K., and M.V. wrote the paper.

The authors declare no conflict of interest.

This article is a PNAS Direct Submission.

Freely available online through the PNAS open access option.

[1]S.C., P.F., and J.H. contributed equally to this work.

[2]To whom correspondence should be addressed. Email: mv245@cam.ac.uk.

This article contains supporting information online at www.pnas.org/lookup/suppl/doi:10.1073/pnas.1700239114/-/DCSupplemental.

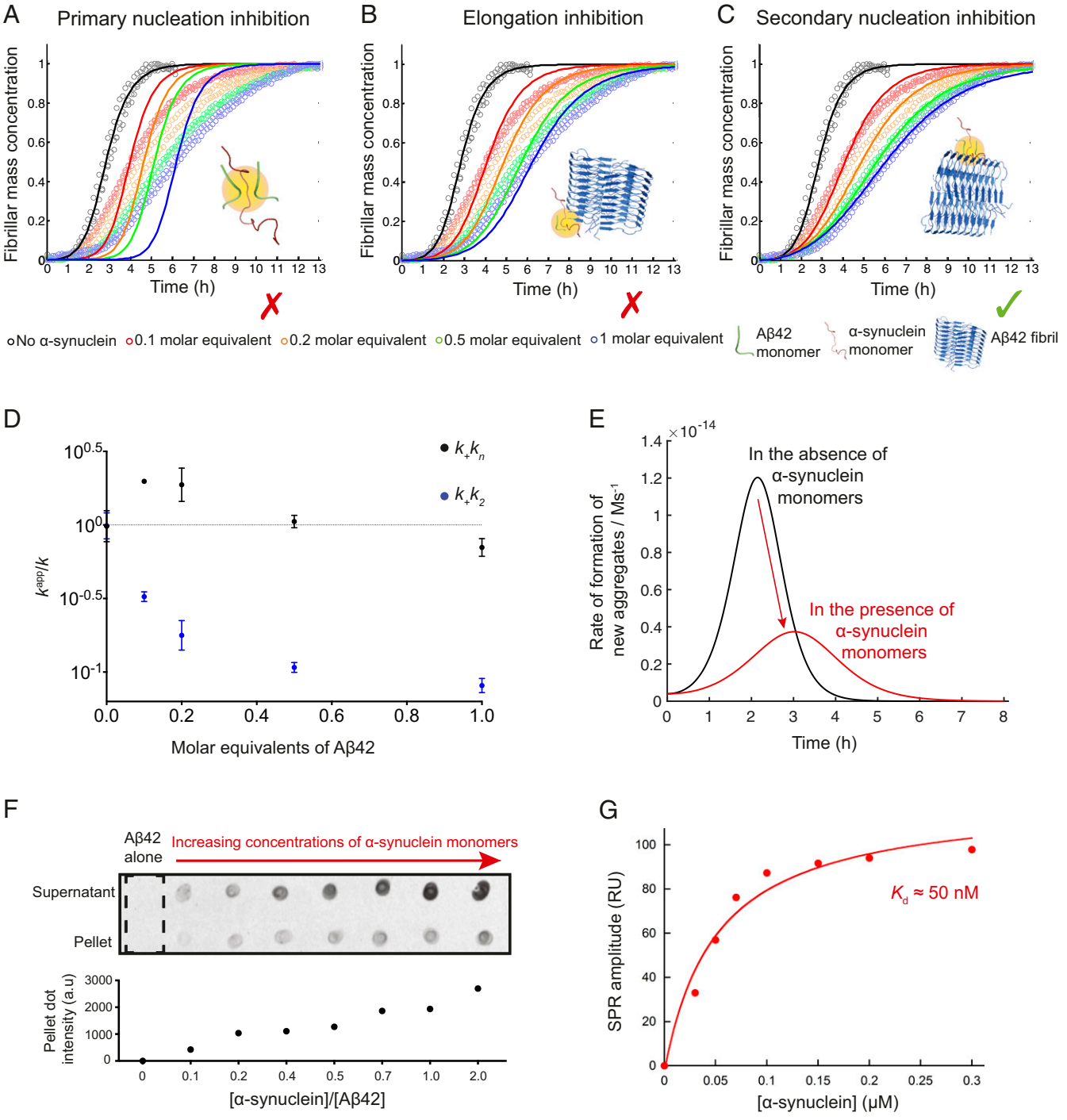

Fig. 1. Monomeric α-synuclein inhibits the secondary nucleation step in Aβ42 aggregation by binding to the surface of Aβ42 fibrils. (*A*–*C*) Kinetic profiles of the aggregation reactions of a 2 μM sample of Aβ42 in the absence and presence of increasing concentrations of α-synuclein monomers (0.2–2 μM, represented by different colors). The solid lines show predictions for the resulting reaction profiles when (*A*) primary nucleation, (*B*) elongation, and (*C*) secondary nucleation are inhibited by α-synuclein monomers. Only the prediction for the case where secondary nucleation is inhibited fits closely the experimental data. (*D*) Evolution of the apparent rate constants from the kinetic analysis in Fig. S1*A* with increasing molar equivalents of α-synuclein monomers (*k* represents in each case k_+k_n or k_+k_2). Note the significant decrease in secondary pathways, k_+k_2, compared with primary pathways, k_+k_n, as the concentration of monomeric α-synuclein increases. Average values were derived from triplicates of each sample in the experiment. (*E*) Numerical simulations of the rate of formation of new Aβ42 aggregates for a 2 μM sample of Aβ42 in the absence (black) or the presence (red) of 0.2 μM monomeric α-synuclein. (*F*) Dot-blot intensities of 5 μM Aβ42 fibrils incubated with increasing concentrations of α-synuclein monomers. A positive correlation between the pellet intensities and α-synuclein shows a likely binding between α-synuclein monomers and Aβ42 fibrils. (*G*) Surface plasmon resonance (SPR) analysis. The equilibrium response (average over three replicates; the SDs are less than the size of the points) is plotted as a function of α-synuclein monomer concentration. The solid line is a fit to a Langmuir isotherm, which estimates an apparent K_d of 50 nM between α-synuclein monomers and Aβ42 fibrils.

monomers can be described by introducing into the rate laws suitable perturbations to each of the microscopic rate constants in the absence and the presence of α-synuclein monomers. The fitting of the aggregation profiles of a 2 μM sample of Aβ42 in the presence of substoichiometric amounts of α-synuclein shows that the experimental data are extremely well described when the surface-catalyzed secondary nucleation rate constant, k_2, is specifically decreased (Fig. 1*C*). On the other hand, predictions based on the alterations of the rate constants of primary nucleation, k_n, and elongation, k_+, are unable to account for the changes in the kinetic curves (Fig. 1 *A* and *B*). Thus, we conclude that monomeric α-synuclein affect specifically secondary pathways (k_2k_+) in the aggregation of Aβ42, with limited effects on primary pathways (k_nk_+) (Fig. 1*D* and Fig. S1*B*).

To strengthen these conclusions, we also carried out an additional set of measurements of the aggregation kinetics of a 2 μM sample of Aβ42 in the presence of 5% preformed Aβ42 fibril seeds. Under these conditions, the primary nucleation step is bypassed and the surface-catalyzed secondary nucleation and elongation steps determine the overall rates of fibril formation. We found that α-synuclein monomers were also able to inhibit the aggregation kinetics under these conditions. The kinetic profiles are described accurately with the master equation using the values of the rate constants k_2 derived from the aggregation reactions in the absence of seeds (Fig. S1*C*).

Monomeric α-Synuclein Suppresses the Proliferation of Aβ42 Aggregates by Binding to Aβ42 Fibrils. Because surface-catalyzed secondary nucleation, which is the dominant mechanism by which Aβ42 proliferates, is responsible for the generation of the large majority of the Aβ42 oligomeric species (24), inhibiting this specific step should have drastic effects on the generation of the oligomers. We found this expectation to be correct, as the rate of formation of new Aβ42 aggregates decreased almost threefold in the presence of as low as 0.1 molar equivalents of α-synuclein monomers (Fig. 1*E*). Moreover, a specific inhibition of the surface-catalyzed secondary nucleation step implies that the inhibitor is likely to bind to the surface of Aβ42 fibrils. Indeed, when increasing concentrations of α-synuclein monomers were incubated with Aβ42 fibrils in a label-free dot-blot assay, an increasing quantity of α-synuclein monomers was found to be associated with Aβ42 fibrils after centrifugation (Fig. 1*F*). Using surface plasmon resonance (SPR) measurements, the interaction between α-synuclein monomers and immobilized Aβ42 fibrils was studied. By fitting to the steady-state response as a function of α-synuclein monomer concentration, the apparent dissociation constant (K_d) was found to be ∼50 nM (Fig. 1*G* and Fig. S1*D*). Note that the aggregation of α-synuclein occurs on a longer timescale with respect to that of Aβ42, especially at the concentration used under our conditions, and hence α-synuclein fibrils are unlikely to be formed under these conditions, as shown from the thioflavin T (ThT) kinetics in Fig. S1*E* (26, 36).

Fibrillar α-Synuclein Introduces a Heterogeneous Nucleation Pathway in Aβ42 Aggregation. When Aβ42 aggregation was performed under seeding conditions, in the presence of preformed α-synuclein fibrils, the aggregation process was found to be accelerated. These results indicate that α-synuclein fibril seeds and Aβ42 fibril seeds have similar effects on Aβ42 aggregation (Fig. 2*A*). The half-times of Aβ42 aggregation reactions gradually decreased with increasing α-synuclein fibril concentrations, even though the seeding ability of α-synuclein fibrils was found to be reduced with respect to that of Aβ42 fibrils (Fig. 2 *B* and *C*). Therefore, we conclude that Aβ42 aggregation is accelerated in the presence of α-synuclein fibrils through a heterogeneous nucleation mechanism (18–20).

The Balance Between Monomeric and Fibrillar Forms of α-Synuclein Determines Its Overall Effect on Aβ42 Aggregation. Taken together, the data presented in this work provide a detailed understanding of the mechanism by which different species of α-synuclein affect the aggregation kinetics of Aβ42. We have shown that, whereas monomeric α-synuclein mainly inhibits the surface-catalyzed secondary nucleation step that is primarily responsible for the generation of Aβ42 fibrils, fibrillar α-synuclein accelerates the reaction through a heterogeneous nucleation mechanism (Fig. 3 *A* and *B*). These findings reveal a complex interplay between nonfibrillar and fibrillar α-synuclein species, which leads to a scenario involving two opposing mechanisms. Calculations derived from the changes in the half-times of the aggregation reactions of Aβ42 that were obtained in the presence of either monomeric or fibrillar species of α-synuclein show that the net effect of a complex mixture containing both monomeric and fibrillar species of α-synuclein on the aggregation of Aβ42 is likely to be strongly dependent on the relative contributions of each of these species (Fig. 3*C* and Fig. S1*F*). Therefore, despite an expected increase in Aβ42 aggregation due to the presence of fibrillar α-synuclein species, the overall aggregation rate of Aβ42 can still decrease due to the inhibitory effect of α-synuclein monomers present in the solution. Specifically, our calculations predict that, for a given concentration of monomeric species of α-synuclein, a higher concentration of the corresponding fibrillar species is required to offset the decrease in the aggregation of Aβ42 (Fig. 3*C*).

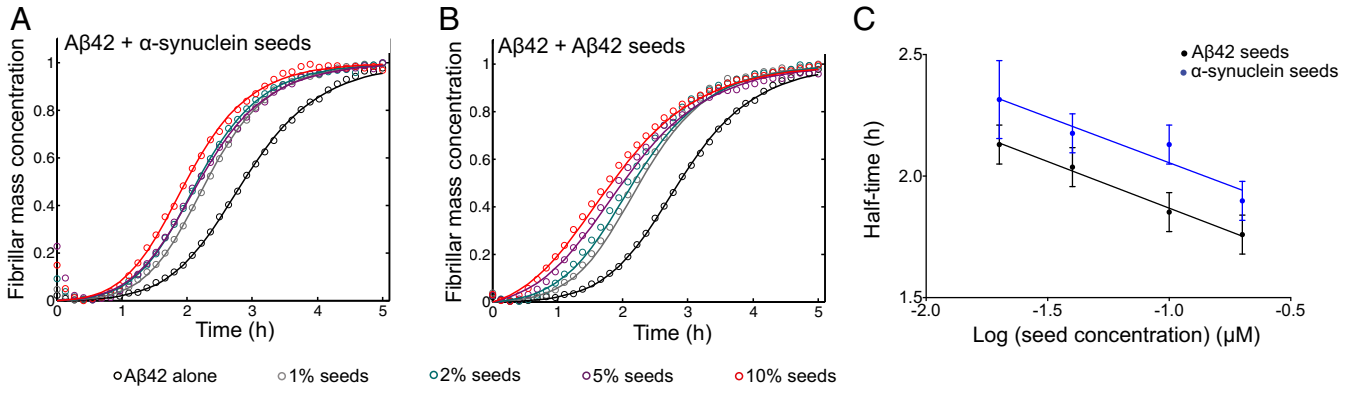

Fig. 2. Fibrillar α-synuclein accelerates the aggregation of Aβ42 through a heterogeneous nucleation process. (*A* and *B*) Kinetic profiles of the aggregation reactions of a 2 μM sample of Aβ42 in the absence and presence of increasing concentrations of preformed (*A*) α-synuclein and (*B*) Aβ42 fibril seeds (represented by different colors). (*C*) Half-times of the aggregation reaction profiles as derived from *A* and *B* as a function of seed concentrations. Average values were derived from triplicates of each sample in the experiment.

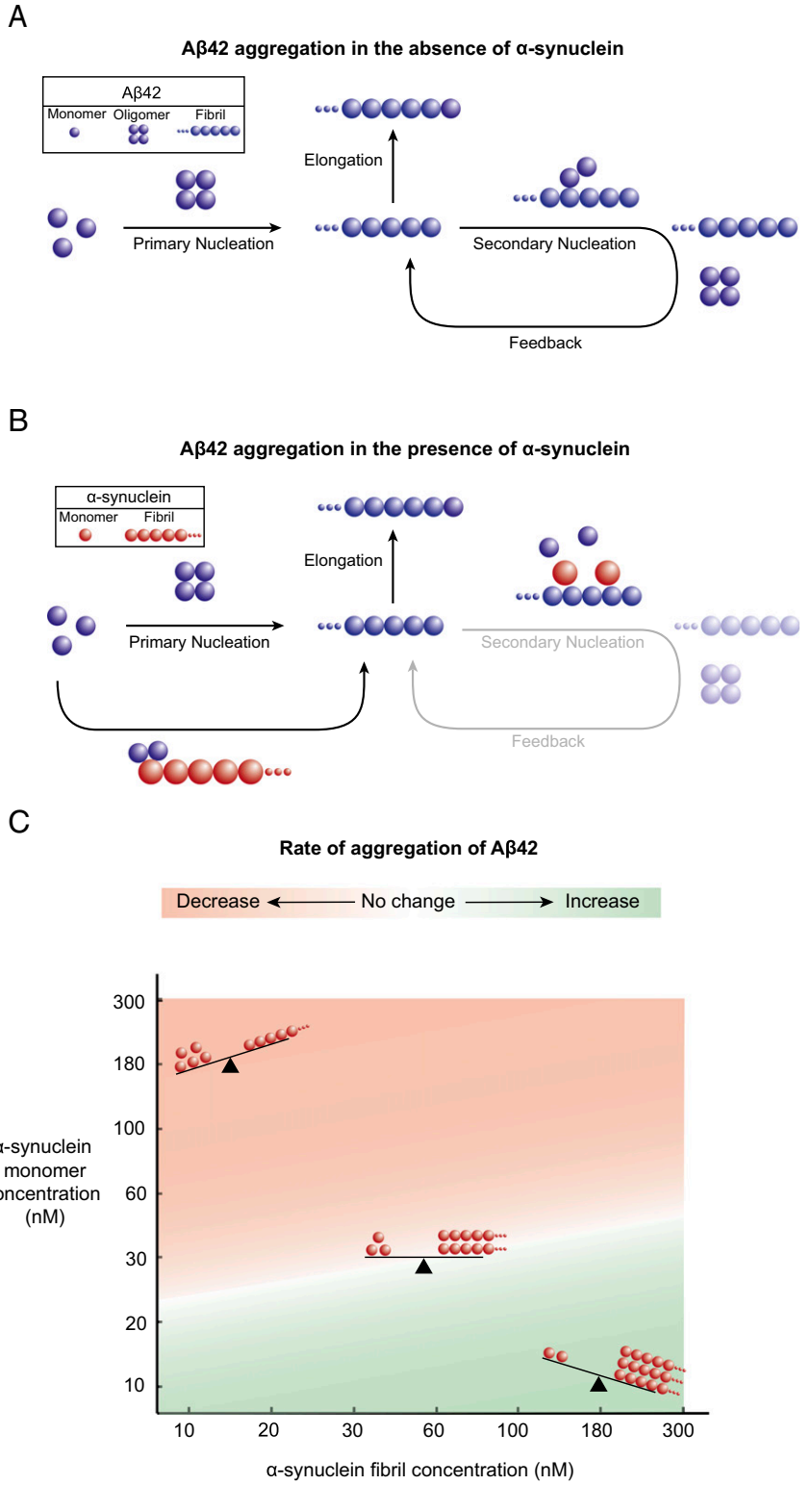

Fig. 3. Schematic representation of the antagonistic effects of fibrillar and monomeric species of α-synuclein on the aggregation kinetics of Aβ42. (*A*) In the absence of α-synuclein, the proliferation of Aβ42 aggregates is dominated by a secondary nucleation pathway, whereby the surfaces of Aβ42 fibrils catalyze the formation of Aβ42 oligomers. (*B*) In the presence of α-synuclein monomers, the secondary nucleation pathway is suppressed, resulting in a decreased rate of the formation of Aβ42 aggregates. Conversely, the presence of α-synuclein fibrils results in an increased rate of the formation of Aβ42 aggregates through a heterogeneous nucleation process. (*C*) Illustration of the complex interplay between α-synuclein monomers and fibrils on the rate of Aβ42 aggregation. The calculations were derived from the changes in the half-times of the aggregation reaction profiles in Fig. S1*F*.

Conclusions

We have shown that the effect of α-synuclein on Aβ42 aggregation depends strongly on the conformational state of α-synuclein. The conformation-dependent effects of α-synuclein on Aβ42 aggregation allow us to reconcile conflicting findings (18–22). These effects also suggest a possible physiological role of α-synuclein by potentially acting as a molecular chaperone capable of inhibiting Aβ42 fibril formation (30). α-Synuclein monomers can exert such a function by binding to Aβ42 fibrils, thereby suppressing surface-catalyzed secondary nucleation. By contrast, α-synuclein fibrils do the opposite by introducing a heterogeneous nucleation pathway. The present findings thus provide insights that could contribute to the development of effective treatments for AD, PD, and DLB based on the inhibition of protein aggregation.

Materials and Methods

Aβ42 and α-Synuclein Preparation. Recombinant Aβ42 and α-synuclein were expressed and purified as described previously (31, 37).

Sample Preparation for Kinetic Experiments. Solutions of monomeric Aβ42 were prepared by dissolving the lyophilized Aβ42 peptide in 6 M GuHCl. Monomeric forms were purified from potential oligomeric species and salt using a Superdex 75 10/300 GL column (GE Healthcare) at a flow rate of 0.5 mL/min, and were eluted in 20 mM sodium phosphate buffer, pH 8, supplemented with 200 μM EDTA and 0.02% NaN_3. The center of the peak was collected and the Aβ42 concentration was determined from the absorbance of the integrated peak area using $\varepsilon_{280} = 1{,}490\ M^{-1}{\cdot}cm^{-1}$. The resulting Aβ42 monomers were diluted with buffer to the desired concentration and supplemented with 20 μM ThT from a 2 mM stock. All samples were prepared in low-binding Eppendorf tubes on ice using careful pipetting to avoid introduction of air bubbles. Each sample was then pipetted into multiple wells of a 96-well half-area, low-binding, clear-bottom, and PEG-coating plate (Corning; 3881), 80 μL per well, in the absence and the presence of different molar equivalents of α-synuclein monomers.

For the preparation of preformed α-synuclein fibrils, 500-μL samples of α-synuclein at concentrations from 500 to 800 μM were incubated in 20 mM phosphate buffer (pH 6.5) for 48–72 h at 40 °C and stirred at 1,500 rpm with a Teflon bar on an RCT Basic Heat Plate (RCT Basic, model no. 0003810002; IKA, Staufen, Germany). Fibrils were diluted to a monomer equivalent concentration of 200 μM, divided into aliquots, flash frozen in liquid N_2, and stored at −80 °C. For the preparation of preformed Aβ42 fibrils, kinetic experiments were set up as above for a 5 μM Aβ42 sample in 20 μM sodium phosphate buffer (pH 8) with 200 μM EDTA and 0.02% NaN_3. Samples were then collected from the wells into low-binding tubes. Preformed fibrils (α-synuclein or Aβ42) were then added to the freshly prepared monomer solution to reach the appropriate final concentration of fibrils.

Kinetic Assays. Assays were initiated by placing the 96-well plate at 37 °C under quiescent conditions in a plate reader (Fluostar Omega, Fluostar Optima, or Fluostar Galaxy; BMGLabtech) (38). The ThT fluorescence was measured through the bottom of the plate with a 440-nm excitation filter and a 480-nm emission filter. The ThT fluorescence was followed for three repeats of each sample.

Theoretical Analysis. The time evolution of the total fibril mass concentration, $M(t)$, is described by the following integrated rate law (23, 24):

$$\frac{M(t)}{M(\infty)} = 1 - \left(\frac{B_+ + C_+}{B_+ + C_+ e^{\kappa t}} \frac{B_- + C_+ e^{\kappa t}}{B_- + C_+}\right)^{\frac{k_\infty^2}{\kappa k_\infty}} e^{-k_\infty t}. \quad [1]$$

To capture the complete assembly process, only two particular combinations of the rate constants define most of the macroscopic behavior. These are related to the rate of formation of new aggregates through primary pathways $\lambda = \sqrt{2k_+k_n m(0)^{n_c}}$ and through secondary pathways $\kappa = \sqrt{2k_+k_2 m(0)^{n_2+1}}$, where the initial concentration of soluble monomers is denoted by $m(0)$, n_c and n_2 describe the dependencies of the primary and secondary pathways on the monomer concentration, and k_n, k_+, and k_2 are the rate constants of the primary nucleation, elongation, and secondary nucleation, respectively.

α-Synuclein can perturb the aggregation process by inhibiting one or more of the individual microscopic reactions. We can identify the microscopic events that are inhibited by α-synuclein monomers by applying the above equation to describe the macroscopic aggregation profiles shown in Fig. 1 *A*–*C* and comparing the set of microscopic rate constants k_+k_n and k_+k_2 required to describe the time evolution of the fibril formation in the absence and presence of α-synuclein monomers. As shown in Fig. 1 *A*–*D*, in unseeded aggregation reactions, the presence of the α-synuclein monomers mainly perturbs the secondary nucleation rate. Fig. S1*C* shows the aggregation profiles of a 5% seeded reaction in the presence of α-synuclein monomers. The fitted lines with the same decrease in k_2 evaluated from the unseeded reaction are also able to describe the decrease in aggregation of the seeded reaction adequately, thus substantiating the fact that α-synuclein monomers are mainly inhibiting the secondary nucleation process.

The numerical simulations reported in Fig. 1*E* show the reaction profiles in the presence and absence of α-synuclein monomer determined according to Eq. **1**. The time evolution of the aggregate formation rate, $r(t)$, was simulated according to the following equation:

$$r(t) = k_2 M(t) m(t)^2 + k_n m(t)^2. \quad [2]$$

The plot in Fig. 3*C* is based on theoretical calculations of the half-time changes of the 2 μM Aβ42 aggregation in the presence of either α-synuclein monomers, or α-synuclein fibrils, as seen from Fig. S1*F*. For this calculation, we assume that, during the course of the aggregation of 2 μM Aβ42 in the presence of both α-synuclein monomers and α-synuclein fibrils, the amount of both α-synuclein monomers and fibrils is constant.

Dot Blot Assay. Blotting was performed using an α-synuclein sequence-specific primary antibody (BD Biosciences). Preformed 5 μM Aβ fibrils were incubated in the absence and presence of 0.1–2 molar equivalents of α-synuclein monomers for 1 h (Fig. 1*F*), and centrifuged at 15,000 rpm for 30 min at 25 °C (RCT Basic, model no. 0003810002; IKA, Staufen, Germany). Pellets and supernatants were then separated, and the pellets were resuspended in the same volume of buffer as that of the supernatant. Two microliters of each pellet and supernatant were spotted onto a nitrocellulose membrane (0.2 μm; Whatman) and then the membranes were dried and then blocked with PBS solution with 5% milk and 0.1% Tween before immune detection. The primary antibody was used according to the manufacturer's instructions. An Alexa Fluor 488-conjugated secondary antibody (Life Technologies) was subsequently added, and fluorescence detection was performed using Typhoon Trio imager (GE Healthcare).

SPR Assays. SPR experiments were performed with a Biacore3000 instrument (GE Healthcare), using CM3 sensors. The carboxylic acid groups on the sensor surface were activated with a mixture of 240 mM EDC and 50 mM NHS to enable standard amine coupling chemistry. A sample of 10 μM monomeric Aβ42, prepared as described above in 20 mM sodium phosphate buffer with 200 μM EDTA, pH 8, was placed in two wells of a 96-well half-area, low-binding, clear-bottom, and PEG-coating plate (Corning; 3881), 100 μL per well, incubated at 37 °C for 1 h, collected into a low-binding 1.5-mL tube (Axygen), and sonicated for 30 s using a sonicator tip and a Soniprep 150 plus sonicator with 1-s pulses at 50% duty cycle for 2 min. The sonicated fibrils were diluted 10-fold in 10 mM NaAc, pH 3, and injected over flow cells 2–4 of the activated the sensor surface for 30 min. All four flow cells were then deactivated by injecting 1 M ethanolamine-HCl, pH 8.5, for 15 min. The cells were rinsed with flow buffer (20 mM sodium phosphate buffer with 200 μM EDTA, pH 8, 0.005% Tween 20) and the Aβ42 fibrils extended by multiple injections of 1 μM Aβ42 in flow buffer, after which the chip was washed overnight with flow buffer. Monomeric α-synuclein was injected over all four channels of the chip for 20 min at concentrations ranging from 0.03 to 0.3 μM followed by buffer flow. The data obtained in flow cell 1 (the blank control) showed no sign of binding to the dextran matrix and was subtracted from the data obtained in the three flow cells with immobilized fibrils. The intensity at the end of the monomer injection was extracted and plotted versus α-synuclein monomer concentration. A Langmuir isotherm was fitted to the data:

$$Y = A * X/(X + K_d),$$

where X is the free monomer concentration, which is assumed to be equal to the injected concentration at equilibrium; A is the signal amplitude at full saturation; and K_d is the equilibrium dissociation constant.

ACKNOWLEDGMENTS. We acknowledge support from the Agency for Science, Technology and Research, Singapore (S.C.); Boehringer Ingelheim Fonds (P.F.); Studienstiftung des Deutschen Volkes (P.F.); the Frances and Augustus Newman Foundation (T.P.J.K.); the UK Biotechnology and Biochemical Sciences Research Council (C.M.D. and M.V.); the Wellcome Trust (C.M.D., T.P.J.K., and M.V.); and the Centre for Misfolding Diseases, University of Cambridge (S.C., P.F., J.H., T.P.J.K., C.M.D., and M.V.).

1. Masters CL, et al. (1985) Amyloid plaque core protein in Alzheimer disease and Down syndrome. *Proc Natl Acad Sci USA* 82:4245–4249.
2. Spillantini MG, et al. (1997) Alpha-synuclein in Lewy bodies. *Nature* 388: 839–840.
3. Knowles TPJ, Vendruscolo M, Dobson CM (2014) The amyloid state and its association with protein misfolding diseases. *Nat Rev Mol Cell Biol* 15:384–396.
4. Eisenberg D, Jucker M (2012) The amyloid state of proteins in human diseases. *Cell* 148:1188–1203.
5. Soto C (2003) Unfolding the role of protein misfolding in neurodegenerative diseases. *Nat Rev Neurosci* 4:49–60.
6. Chiti F, Dobson CM (2006) Protein misfolding, functional amyloid, and human disease. *Annu Rev Biochem* 75:333–366.
7. Aguzzi A, O'Connor T (2010) Protein aggregation diseases: Pathogenicity and therapeutic perspectives. *Nat Rev Drug Discov* 9:237–248.
8. Haass C, Selkoe DJ (2007) Soluble protein oligomers in neurodegeneration: Lessons from the Alzheimer's amyloid beta-peptide. *Nat Rev Mol Cell Biol* 8:101–112.
9. Benilova I, Karran E, De Strooper B (2012) The toxic Aβ oligomer and Alzheimer's disease: An emperor in need of clothes. *Nat Neurosci* 15:349–357.
10. Lotharius J, Brundin P (2002) Pathogenesis of Parkinson's disease: Dopamine, vesicles and α-synuclein. *Nat Rev Neurosci* 3:932–942.
11. Lashuel HA, Overk CR, Oueslati A, Masliah E (2013) The many faces of α-synuclein: From structure and toxicity to therapeutic target. *Nat Rev Neurosci* 14:38–48.
12. Silva BA, Breydo L, Uversky VN (2013) Targeting the chameleon: A focused look at α-synuclein and its roles in neurodegeneration. *Mol Neurobiol* 47:446–459.
13. Takeda A, et al. (1998) Abnormal accumulation of NACP/α-synuclein in neurodegenerative disorders. *Am J Pathol* 152:367–372.
14. Hamilton RL (2000) Lewy bodies in Alzheimer's disease: A neuropathological review of 145 cases using alpha-synuclein immunohistochemistry. *Brain Pathol* 10:378–384.
15. Uéda K, et al. (1993) Molecular cloning of cDNA encoding an unrecognized component of amyloid in Alzheimer disease. *Proc Natl Acad Sci USA* 90:11282–11286.
16. Walker Z, Possin KL, Boeve BF, Aarsland D (2015) Lewy body dementias. *Lancet* 386: 1683–1697.
17. Stinton C, et al. (2015) Pharmacological management of Lewy body dementia: A systematic review and meta-analysis. *Am J Psychiatry* 172:731–742.
18. Yoshimoto M, et al. (1995) NACP, the precursor protein of the non-amyloid β/A4 protein (Aβ) component of Alzheimer disease amyloid, binds Aβ and stimulates Aβ aggregation. *Proc Natl Acad Sci USA* 92:9141–9145.
19. Jensen PH, et al. (1997) Binding of Abeta to α- and β-synucleins: Identification of segments in α-synuclein/NAC precursor that bind Abeta and NAC. *Biochem J* 323:539–546.
20. Ono K, Takahashi R, Ikeda T, Yamada M (2012) Cross-seeding effects of amyloid β-protein and α-synuclein. *J Neurochem* 122:883–890.
21. Bachhuber T, et al. (2015) Inhibition of amyloid-β plaque formation by α-synuclein. *Nat Med* 21:802–807.
22. Kallhoff V, Peethumnongsin E, Zheng H (2007) Lack of α-synuclein increases amyloid plaque accumulation in a transgenic mouse model of Alzheimer's disease. *Mol Neurodegener* 2:6.
23. Cohen SIA, Vendruscolo M, Dobson CM, Knowles TPJ (2012) From macroscopic measurements to microscopic mechanisms of protein aggregation. *J Mol Biol* 421:160–171.
24. Cohen SIA, et al. (2013) Proliferation of amyloid-β42 aggregates occurs through a secondary nucleation mechanism. *Proc Natl Acad Sci USA* 110:9758–9763.
25. Meisl G, et al. (2016) Molecular mechanisms of protein aggregation from global fitting of kinetic models. *Nat Protoc* 11:252–272.
26. Flagmeier P, et al. (2016) Mutations associated with familial Parkinson's disease alter the initiation and amplification steps of α-synuclein aggregation. *Proc Natl Acad Sci USA* 113:10328–10333.
27. Meisl G, et al. (2014) Differences in nucleation behavior underlie the contrasting aggregation kinetics of the Aβ40 and Aβ42 peptides. *Proc Natl Acad Sci USA* 111:9384–9389.
28. Cohen SIA, et al. (2015) A molecular chaperone breaks the catalytic cycle that generates toxic Aβ oligomers. *Nat Struct Mol Biol* 22:207–213.
29. Månsson C, et al. (2014) Interaction of the molecular chaperone DNAJB6 with growing amyloid-beta 42 (Aβ42) aggregates leads to sub-stoichiometric inhibition of amyloid formation. *J Biol Chem* 289:31066–31076.
30. Arosio P, et al. (2016) Kinetic analysis reveals the diversity of microscopic mechanisms through which molecular chaperones suppress amyloid formation. *Nat Commun* 7:10948.
31. Habchi J, et al. (2016) An anticancer drug suppresses the primary nucleation reaction that initiates the production of the toxic Aβ42 aggregates linked with Alzheimer's disease. *Sci Adv* 2:e1501244.
32. Habchi J, et al. (2017) Systematic development of small molecules to inhibit specific microscopic steps of Aβ42 aggregation in Alzheimer's disease. *Proc Natl Acad Sci USA* 114:E200–E208.
33. Aprile FA, et al. (2017) Selective targeting of primary and secondary nucleation pathways in Aβ42 aggregation using a rational antibody scanning method. *Sci Adv* 3(6):e1700488.
34. Arosio P, Vendruscolo M, Dobson CM, Knowles TPJ (2014) Chemical kinetics for drug discovery to combat protein aggregation diseases. *Trends Pharmacol Sci* 35:127–135.
35. Knowles TPJ, et al. (2009) An analytical solution to the kinetics of breakable filament assembly. *Science* 326:1533–1537.
36. Galvagnion C, et al. (2015) Lipid vesicles trigger α-synuclein aggregation by stimulating primary nucleation. *Nat Chem Biol* 11:229–234.
37. Hoyer W, et al. (2002) Dependence of α-synuclein aggregate morphology on solution conditions. *J Mol Biol* 322:383–393.
38. Hellstrand E, Boland B, Walsh DM, Linse S (2010) Amyloid β-protein aggregation produces highly reproducible kinetic data and occurs by a two-phase process. *ACS Chem Neurosci* 1:13–18.

Supporting Information

Chia et al. 10.1073/pnas.1700239114

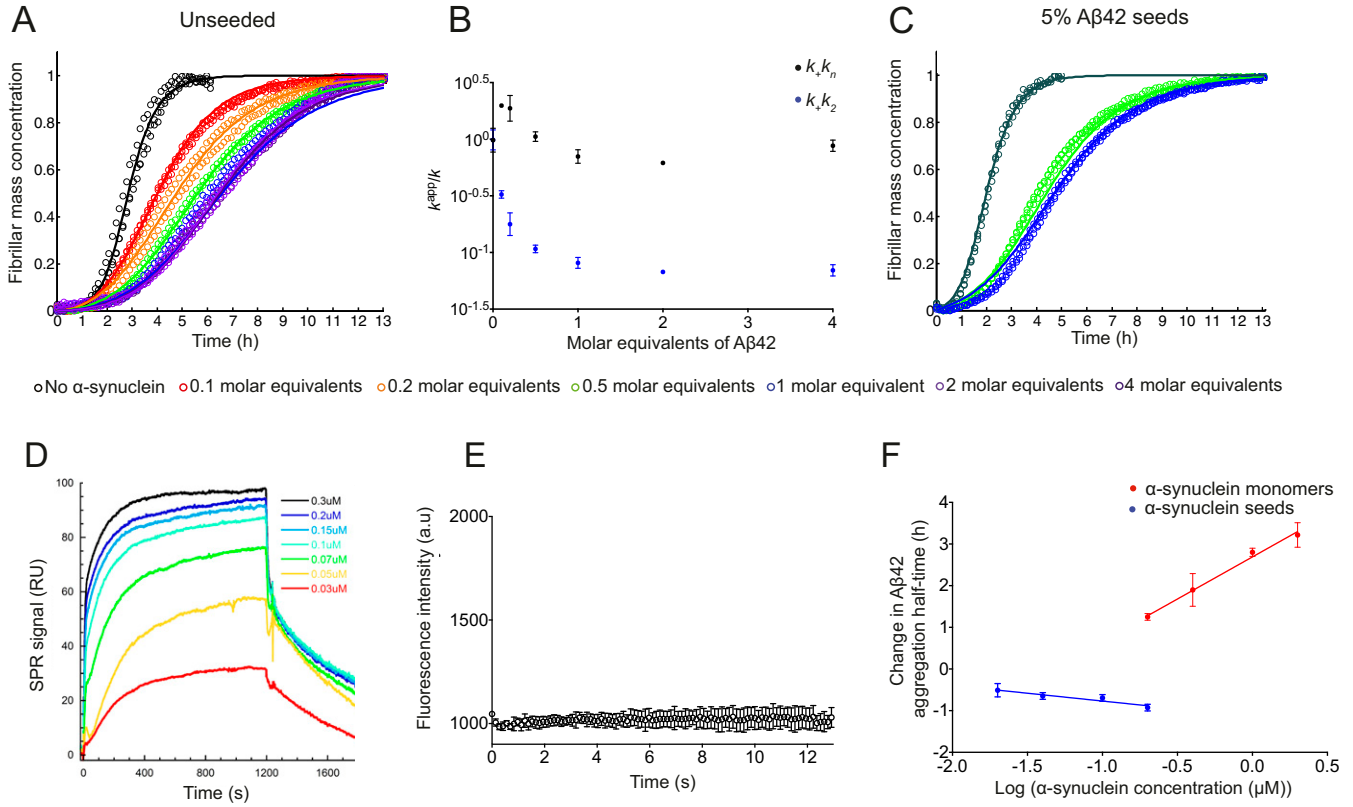

Fig. S1. Effects of monomeric and fibrillar species of α-synuclein on the aggregation kinetics of Aβ42. (*A*) Kinetic profiles of the aggregation reactions of a 2 μM sample of Aβ42 in the absence and the presence of increasing concentrations of α-synuclein monomers (represented by different colors). The inhibitory effect saturates at a critical concentration, corresponding approximately to 2 molar equivalents with respect to Aβ42. The solid lines show predictions for the resulting reaction profiles with changes in both k_+k_n and k_+k_2. k_n is the rate of primary nucleation, k_+ is the rate of elongation, and k_2 is the rate of secondary nucleation. (*B*) Evolution of the apparent rate constants from predictions in *A* with increasing concentration ratios of α-synuclein monomers (k represents in each case k_+k_n or k_+k_2). Note the significant decrease in secondary pathways, k_+k_2, compared with primary pathways, k_+k_n, as the concentration of α-synuclein monomer increases. At over stoichiometric amounts of α-synuclein, an additional limited contribution could also come from the binding to ends of Aβ fibrils. (*C*) Kinetic profiles of the aggregation reactions of a 2 μM sample of Aβ42 in the presence of 5% of preformed seeds and in the absence (dark green) and presence of 0.5 (green) and 1 molar equivalent (blue) of α-synuclein monomer. The solid lines show predictions for the reaction profiles, with the rate constants derived from the experiments performed in the absence of seeds (*B*). The same decrease in k_2 as obtained from the unseeded data in the presence of α-synuclein monomer also describes the kinetic curves in the presence of 5% fibril seeds. (*D*) Sensorgrams showing the response recorded as a function of time during 1,200-s injections of increasing concentrations of α-synuclein monomers over a sensor with immobilized Aβ42 fibrils. (*E*) ThT fluorescence measurements of 4 μM α-synuclein monomers alone over time. Note that no significant increase in ThT could be detected over the course of 13 h. (*F*) Changes in the half-times of Aβ42 aggregation reactions in the presence of increasing concentrations of α-synuclein monomers (in orange) and α-synuclein fibrils (in blue), as derived from *A* and Fig. 2*A*.